Processing and Application of Ceramics 11 [3] (2017) 191–200
https://doi.org/10.2298/PAC1703191C

Structure and electrical properties of $Ba(In_{0.5}Nb_{0.5})_{1-x}Ti_xO_3$ ceramics

Kumar P. Chandra[1], Ajit R. Kulkarni[2], Priyanka[3], Kamal Prasad[3,*]

[1]*Department of Physics, S.M. College, Bhagalpur - 812001, India*
[2]*Department of Metallurgical Engineering and Materials Science, Indian Institute of Technology, Mumbai - 400076, India*
[3]*Materials Research Laboratory, University Department of Physics, T. M. Bhagalpur University, Bhagalpur - 812007, India*

Received 8 April 2017; Received in revised form 25 July 2017; Accepted 23 August 2017

Abstract

Lead-free $Ba(In_{0.5}Nb_{0.5})_{1-x}Ti_xO_3$ ($0 \leq x \leq 1$) ceramics was synthesized using a standard high temperature solid-state reaction method and sintered at 1400 °C/4 h (except the pure $BaTiO_3$ which was sintered at 1300 °C/4 h). The ceramics was characterized by X-ray diffraction, scanning electron microscopy, dielectric, impedance and AC conductivity studies. The crystal structure of the compounds was found to be cubic (with the space group Pm3m) for x = 0, 0.25 and 0.50 and tetragonal (P4/mmm) for x = 0.75 and 1.0. Increase in Ti-content in the ceramic samples leads to the decrease in unit cell volume while the values of real as well as imaginary parts of dielectric constant and AC conductivity increase. Complex impedance spectroscopy analysis indicated the negative temperature coefficient of resistance. AC conductivity data supported the hopping type of conduction in the system and obeyed Jonscher's power law. The real and imaginary parts of dielectric constant and AC conductivity data fit excellently well with an exponential function.

Keywords: *$Ba(In_{0.5}Nb_{0.5})_{1-x}Ti_xO_3$, perovskite structure, electrical and dielectric properties*

I. Introduction

Lead-bearing compounds with perovskite ABO_3-type structures are widely used for capacitor, pyroelectric, piezoelectric, electro-optic, magneto-electric applications. Currently, immense interest is being shown worldwide by the academia as well as industries either eliminate or minimize the use of hazardous substances such as lead in the electrical/electronic equipment due to the fact that electronic gadgets containing lead are not recyclable and are listed as toxic. Besides, different principles of chemistry (e.g. ionic radii, valence state, tolerance factor, etc.) when combined together result in formulation of numerous complex perovskite oxides having the mixed-cation formula such as $(A'A''\ldots)BO_3$, $A(B'B''\ldots)O_3$ or $(A'A''\ldots)(B'B''\ldots)O_3$ with variety of interesting properties which find many industrial applications [1–5]. It has been observed that modifications either at A- or B-site are very important in tailoring various properties of complex perovskites. Thus, the size difference of pseudo-cation $(A'A''\ldots)^{2+}$ and/or $(B'B''\ldots)^{4+}$ and difference of their valance states play important role.

$BaTiO_3$ is a well-known ferroelectric material with perovskite type tetragonal (*P4/mmm*) structure (tolerance factor 0.9972). It has found widespread applications as a capacitor material because of its high permittivity ($\sim 10^3$). There are enormous literature data on the homovalent, heterovalent ions doped $BaTiO_3$ either at Ba and/or Ti-site or at both sites, and solid solution of $BaTiO_3$ with other perovskite materials, which showed promising electrical behaviour [6–12]. On the other hand, $Ba(In_{0.5}Nb_{0.5})O_3$ with cubic (*Pm3m*) structure [13,14] (tolerance factors: 0.9934) is very stable material with low dielectric constant (~45) and loss tangent ($\sim 10^{-2}$) and it has been considered as a good candidate for microwave applications [15]. Furthermore, with the aim of getting lead-free compounds suitable for device application, attempts have been made to modify Ti-site by the pseudo-tetravalent cation $(B,Nb)^{4+}$, where B is trivalent ion. Thus, the electrical properties of a number of solid-solutions, such as: $Ba(Fe_{0.5}Ta_{0.5})O_3$ [8], $Ba(Fe_{0.5}Nb_{0.5})O_3$

* Corresponding author: tel/fax: +91 641 2501699,
e-mail: *k.prasad65@gmail.com*

[16–19], $Ba(Sm_{0.5}Nb_{0.5})O_3$ [20], $Ba(Y_{0.5}Nb_{0.5})O_3$ [21], $Ba(Bi_{0.5}Ta_{0.5})O_3$ [22], $Ba(Co_{0.5}W_{0.5})O_3$ [23], $Ba(Zn_{0.5}W_{0.5})O_3$ [24], with $BaTiO_3$ have been reported recently. Also, extensive literature survey suggested that no attempt has been made so far on (1-x) $Ba(In_{0.5}Nb_{0.5})O_3$–x $BaTiO_3$ ($0 \leq x \leq 1$) solid-solutions. Both $BaTiO_3$ and $Ba(In_{0.5}Nb_{0.5})O_3$ are described as typical perovskite-type compounds and could be expected to form solid solutions. Therefore, it is of great interest to study the structural and electrical properties of $Ba(In_{0.5}Nb_{0.5})_{1-x}Ti_xO_3$ ceramics. Accordingly, studies on the structure and electrical properties of $Ba(In_{0.5}Nb_{0.5})_{1-x}Ti_xO_3$ (abbreviated hereafter as BINT) ceramics with different composition (x = 0, 0.25, 0.50, 0.75 and 1.0) were performed in this work. Further, an attempt was made to understand the dielectric relaxation and electrical conduction mechanism in the system using complex impedance spectroscopy technique. Also, a mathematical model was proposed to explain the real and imaginary parts of dielectric constant and AC conductivity data.

II. Materials and methods

Polycrystalline $Ba(In_{0.5}Nb_{0.5})_{1-x}Ti_xO_3$ samples (where x = 0, 0.25, 0.50, 0.75 and 1.0) samples were prepared using $BaCO_3$, In_2O_3, Nb_2O_5 and TiO_2 (with AR grade 99.9%, Merck) in proper stoichiometric proportions and by single step solid-state reaction process according to the thermo-chemical reaction:

$$BaCO_3 + \left(\frac{1-x}{4}\right)In_2O_3 + \left(\frac{1-x}{4}\right)Nb_2O_5 + xTiO_2 \xrightarrow{\Delta}$$
$$Ba(B_{0.5}Nb_{0.5})_{1-x}Ti_xO_3 + CO_2(g)\uparrow$$

The reaction was carried out at 1350 °C for 5 h in air atmosphere, except for $BaTiO_3$ (x = 1.0) which was kept at 1250 °C for 5 h. The calcined powders were then ground and uniaxially pressed at ~650 MPa to form pellets having thickness of 1.5–2 mm and diameter of 9.5–10 mm. Polyvinyl alcohol (PVA) was used as binder. The pellets were subsequently sintered at 1400 °C/4 h, except for the pure $BaTiO_3$ for which it was 1300 °C/4 h. The completion of reactions and the formation of desired compounds were checked by X-ray diffraction (XRD) technique. The weights of the samples were monitored before and after the heat treatments. The maximum difference was noted to be about 1.08 mg for the total of 10 g of the samples. Therefore, the compositions of the samples were considered to be the same as the initial one.

The crystal structure was identified using XRD analyses with CuKα radiation (X'PERT-PRO, Pan Analytical) for all the sintered specimens. The XRD data for Rietveld analysis were collected over the range of 2θ = 25–80° with a step size of 0.02° and a count time of 2 s. The FullProf program was used for Rietveld structural refinement. The Bragg peaks were modelled with pseudo-Voigt function and the backgrounds were estimated by linear interpolation between selected background points. The microstructure of all the specimens was obtained by a scanning electron microscopy (SEM Hitachi S-3400N, Japan) on the fractured surface. For electrical characterization, the samples were polished and air drying silver paste (SPI, Structure Probe, Inc.) was applied on both surfaces of the samples to serve as electrodes. The real and imaginary parts of the electrical impedance were measured as a function of frequency (1 Hz $\leq f \leq$ 1 MHz) between 50 and 450 °C at a heating rate of 1 °C/min with a computer interfaced Solartron SI1260 impedance/gain phase analyser. AC conductivity data were calculated using the relation $\sigma_{AC} = 2\pi \cdot f \cdot \varepsilon_0 \cdot \varepsilon' \cdot \tan\delta$, where f is frequency, ε' is the real part of the dielectric constant and $\tan\delta$ is dielectric loss. Further, the temperature coefficient of capacitance (T_{CC}) which is an important parameter for the low-temperature dependence of capacitance was obtained using the relation:

Table 1. The crystal data and refinement factors of $Ba(In_{0.5}Nb_{0.5})_{1-x}Ti_xO_3$ ceramics (x = 0, 0.25, 0.50, 0.75 and 1.0) ceramics obtained from X-ray powder diffraction data

Composition, x	0	0.25	0.5	0.75	1
Crystal System	Cubic	Cubic	Cubic	Tetragonal	Tetragonal
Space group	*Pm3m*	*Pm3m*	*Pm3m*	*P4/mmm*	*P4/mmm*
a [Å]	4.1413	4.1093	4.0693	4.0172	3.9912
c [Å]	-	-	-	4.0214	4.0264
V [Å^3]	71.0272	69.3912	67.3819	64.8982	64.1401
Profile factor, R_p	25.4	26.8	27.2	23.5	37.1
Weighted profile factor, R_{wp}	23.7	25.3	25.5	25.2	37.9
Expected weighted profile factor, R_{exp}	14.2	14.4	15.3	16.2	16.6
Bragg factor, R_B	0.223×10^{-3}	0.239×10^{-3}	0.492×10^{-3}	0.0810	0.0242
Crystallographic R_F factor	0.210×10^{-3}	0.330×10^{-3}	0.661×10^{-3}	0.166	0.0259
χ^2	2.778	3.084	2.780	2.42	5.22
Durbin-Watson statistics, d	0.7425	0.6962	0.8244	1.8348	0.6712
Q_D	1.8980	1.8960	1.8966	1.8584	1.9082
Goodness of fit S	1.6690	1.7569	1.6667	1.5556	2.28

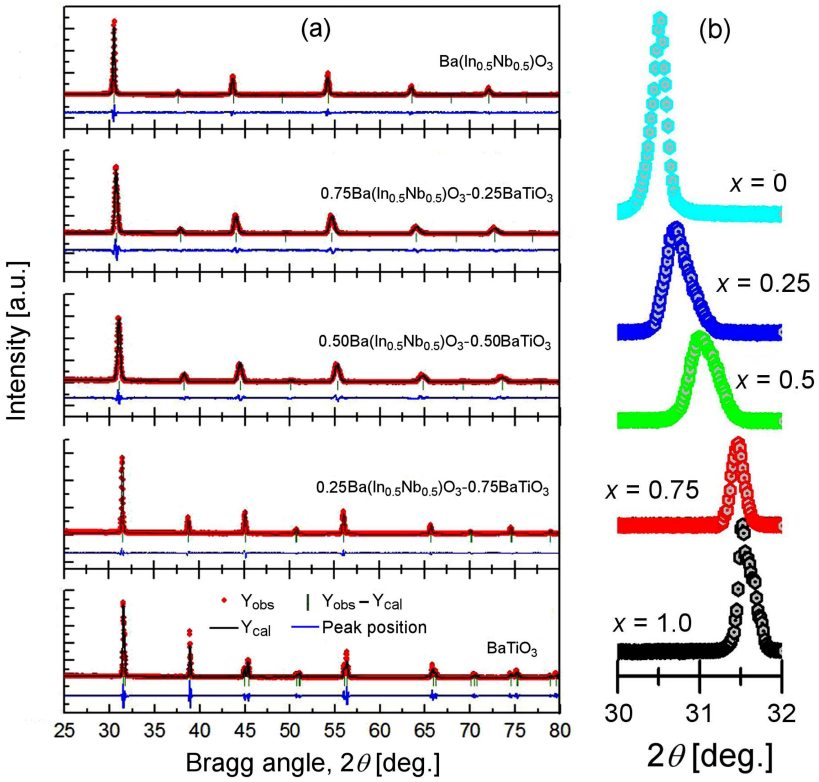

Figure 1. (a) Rietveld refined patterns of $Ba(In_{0.5}Nb_{0.5})_{1-x}Ti_xO_3$ ceramics (symbols represent the observed data points, solid lines their Rietveld fit, vertical lines their Bragg positions and lower solid lines their difference between the observed-calculated data) and (b) X-ray diffraction patterns of selected regions (2θ range 30°–32°)

$$T_{CC} = \frac{\varepsilon'_T - \varepsilon'_{RT}}{\varepsilon'_{RT}} \cdot 100 \qquad (1)$$

where ε'_T and ε'_{RT} are real parts of dielectric constant at elevated and room temperature, respectively.

III. Results and discussion

Rietveld refinement of XRD data of $Ba(In_{0.5}Nb_{0.5})_{1-x}Ti_xO_3$ (BINT, where x = 0, 0.25, 0.50, 0.75 and 1.0) were carried out to see the effect of pseudo-cation $(In_{0.5}{}^{3+},Nb_{0.5}{}^{5+})^{4+}$ addition to $BaTiO_3$ on its unit cell structure. Figure 1a shows the observed, calculated and difference profiles for the BINT ceramics after the refinements. The appearance of single and sharp peaks of perovskite phase and no other peaks of any oxides and/or carbonates indicated the formation of single phase compounds. It can also be seen that the profiles for the observed and calculated ones are perfectly matching. The adopted profile fitting procedure was minimizing the χ^2 function. The crystal data and refinement parameters of the BINT are depicted in Table 1. The compounds show a single cubic phase formation with space group *Pm3m* except for x = 0.75 and 1.0 for which the unit cell structure comes out to be tetragonal (*P4/mmm*). Therefore, the addition of pseudo-cation $(In_{0.5}{}^{3+},Nb_{0.5}{}^{5+})^{4+}$ to $BaTiO_3$ changes the basic unit cell structure of the solid-solutions for $x \geq 0.75$. This could be due to the highly tolerant $Ba(In_{0.5}Nb_{0.5})O_3$ structure (tolerance factor ~1). However, shifting in the peak positions and changes in the intensities of peaks could be observed with the increase in the value of x. The shift in diffraction peaks towards higher Bragg's angle indicated the decrease in lattice parameters with increasing x (Fig. 1b). Furthermore, it is observed that the unit cell volume decreases with increasing x, which could be due to the partial replacement of pseudo-cation $(In_{0.5}{}^{3+},Nb_{0.5}{}^{5+})^{4+}$ with Ti^{4+}. A second order polynomial fitting to concentration (x) dependence of unit cell volume data yielded a relation:

$$V = 71.20422 - 8.77134 \cdot x + 1.46446 \cdot x^2 \qquad (2)$$

with $r^2 = 0.9696$.

Figure 2 shows the SEM micrographs of the fractured surface of the sintered BINT ceramics. The characteristic polycrystalline texture can be recognised as well as the presence of a very small amount of pores suggesting high density of the samples. The grains of unequal sizes (1–4 μm) were found for the chosen compositions. It is also observed that a few grains are larger in comparison to the average size which can be termed as an abnormal grain growth.

The frequency dependence of real (ε') and imaginary (ε'') parts of dielectric constant for the BINT ceramics at different temperatures are shown in Figs. 3 and 4, respectively. It is observed that the values of both ε' and ε'' decrease with increasing frequency. A relatively

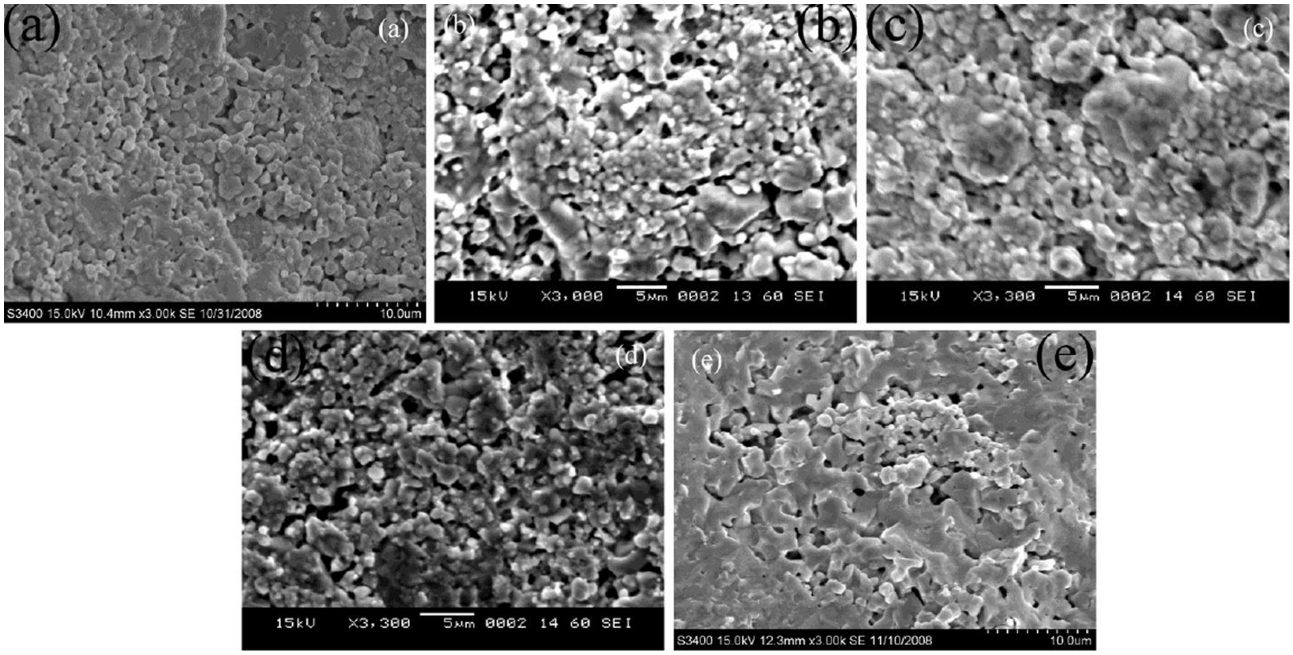

Figure 2. SEM micrographs of $Ba(In_{0.5}Nb_{0.5})_{1-x}Ti_xO_3$ ceramics: a) $x = 0$, b) $x = 0.25$, c) $x = 0.50$, d) $x = 0.75$ and e) $x = 1.0$

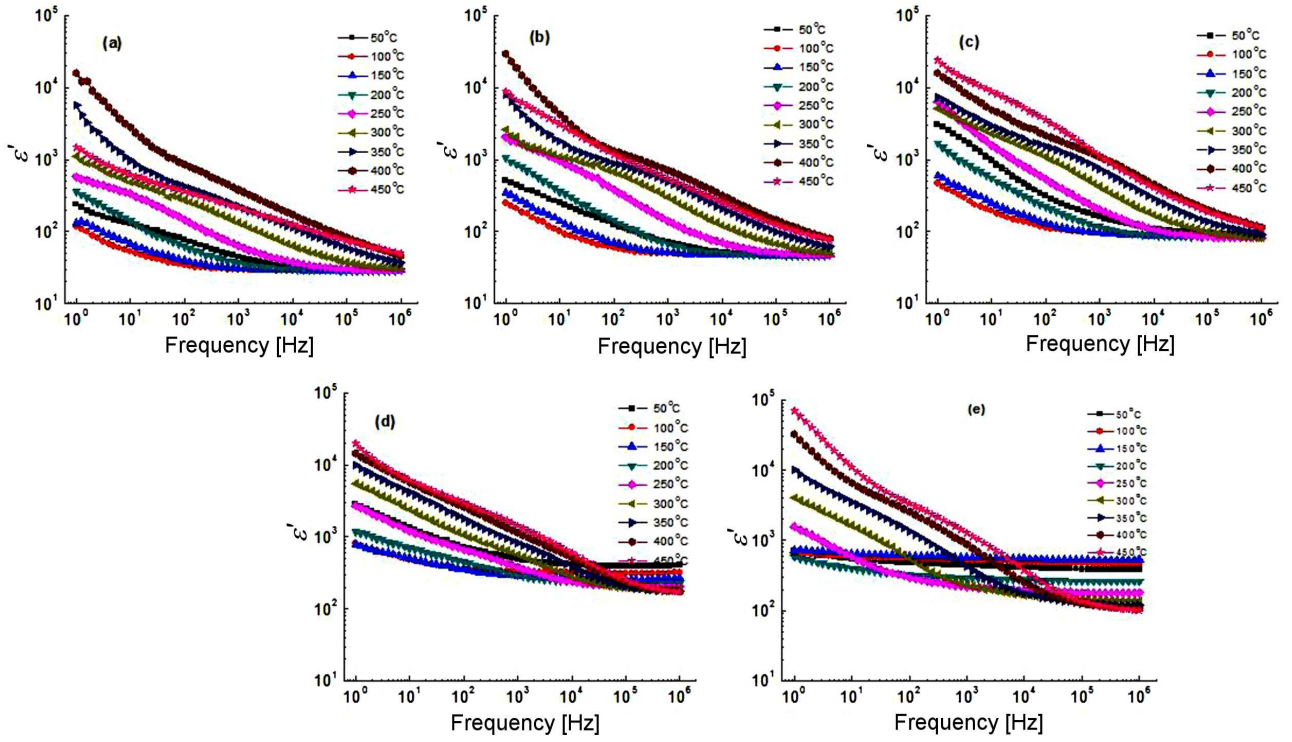

Figure 3. Variation of real part of dielectric constant with frequency of $Ba(In_{0.5}Nb_{0.5})_{1-x}Ti_xO_3$ ceramics: a) $x = 0$, b) $x = 0.25$, c) $x = 0.50$, d) $x = 0.75$ and e) $x = 1.0$ at different temperatures

high dielectric constant at low frequencies and its fast decreases at high frequencies are characteristic of almost all dielectric materials. These are due to the fact that dipoles can be moved easily at low frequencies, but cannot follow the field at high frequencies. It is known that the variations in ε' and ε'' are attributed to the different types of polarizations, e.g. ionic, electronic, dipolar and space charge or interfacial which arise at different stages of material's response on varying temperature and frequency of the applied alternating field. Each of these involves a short range displacement of charges and contributes to the total polarization and hence to the permittivity of the material.

The temperature variation of ε' and ε'' for the BINT ceramics at different frequencies are illustrated in Fig. 5. The values of both ε' and ε'' were found almost insensitive up to 100 °C ($T_{CC} \sim \pm 10\%$) and then they start increasing with the further rise in temperature except in

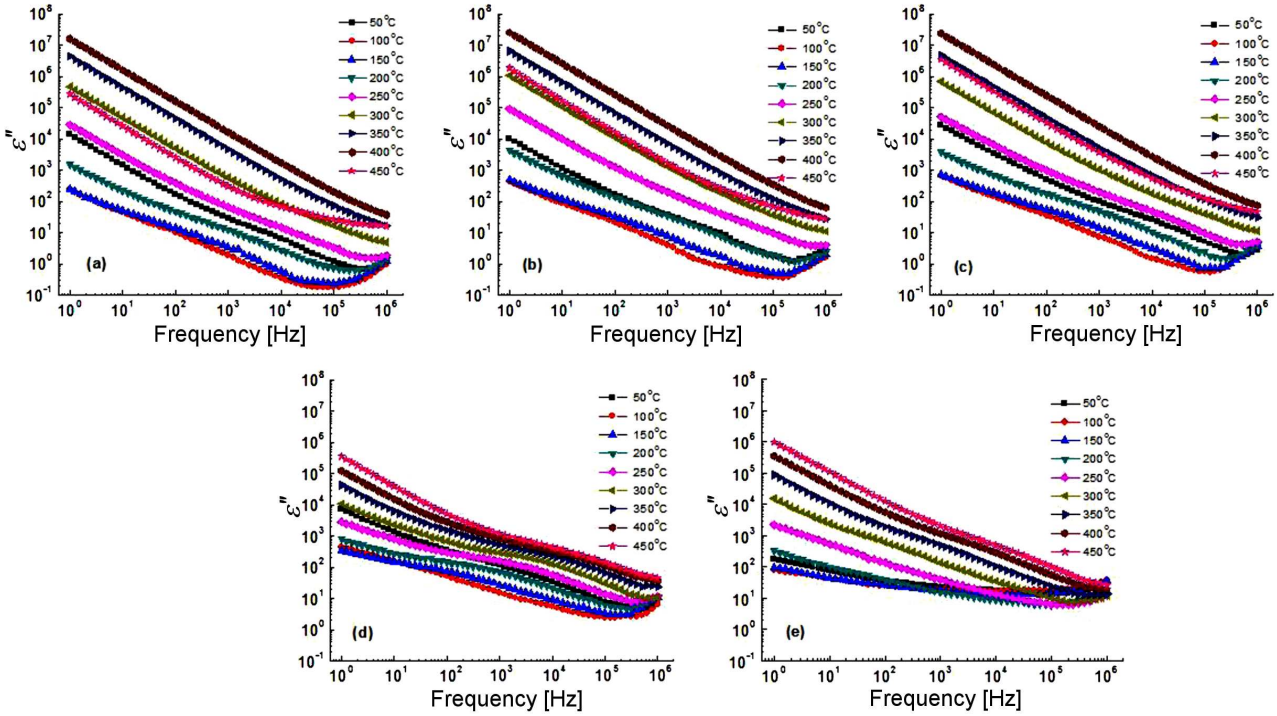

Figure 4. Variation of imaginary part of dielectric constant with frequency of $Ba(In_{0.5}Nb_{0.5})_{1-x}Ti_xO_3$ ceramics: a) $x = 0$, b) $x = 0.25$, c) $x = 0.50$, d) $x = 0.75$ and e) $x = 1.0$ at different temperatures

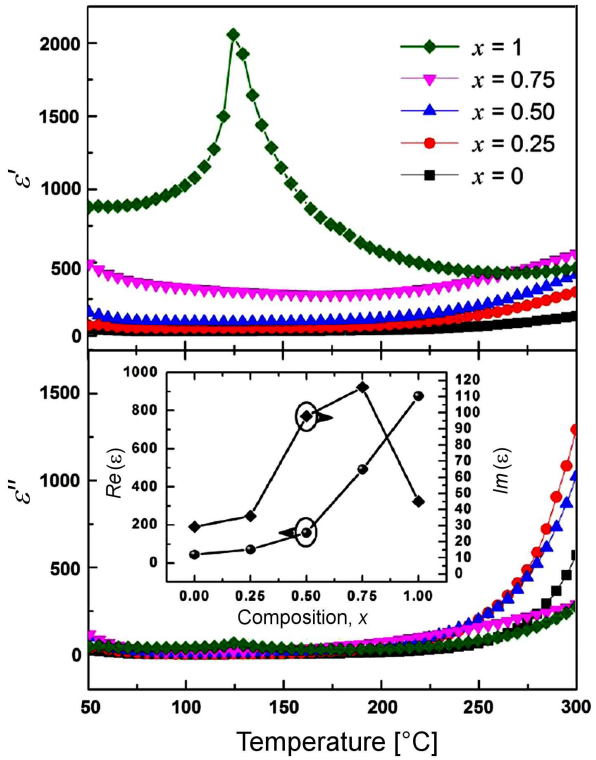

Figure 5. Variation of the real and imaginary parts of dielectric constant with temperature at 1 kHz of $Ba(In_{0.5}Nb_{0.5})_{1-x}Ti_xO_3$ ($x = 0$, 0.25, 0.50, 0.75 and 1.0) ceramics. Inset: Compositional dependence of the real and imaginary parts of dielectric constant at 1 kHz and room temperature

the case of the pure $BaTiO_3$ for which ε'-T as well as ε''-T plots have a maximum at ~120 °C. Inset in Fig. 5 shows the compositional dependence of ε' and ε'' for the BINT ceramics at room temperature and 1 kHz. It can be seen that ε' simply increase with the increment in $BaTiO_3$ content (x) while ε'' find a maximum for x = 0.75. Hence, addition of $BaTiO_3$ to $Ba(In_{0.5}Nb_{0.5})O_3$ is advantageous for capacitor applications, especially for x = 0.50.

The logarithmic frequency dependence of Z' and Z'' of the BINT, at different temperatures are plotted in Figs. 6 and 7, respectively. It is observed that Z' decreases monotonically with increasing frequency for all temperatures. On the other hand, Z'' decreases monotonically only at lower temperatures suggesting the absence of any relaxation. This suggests that the relaxation species are immobile defects and the orientation effect might be associated. At higher temperatures, the peak in Z''-f plots appears (Fig. 7), and shifts towards higher frequency with the increment in temperature showing that the resistance of the bulk material is decreasing and supports NTCR character of the BINT. Upon further rise in temperature Z''-f plots exhibited double peaks, which clearly indicated the introduction of grain boundary effect especially in case of the sample with $x \geq 0.75$. Besides, the magnitude of Z'' peaks decreases while the width of the peak increases with increasing temperature and the peaks are slightly asymmetric in nature for all the compounds. This suggests that there is a spread of relaxation times, i.e. the existence of a temperature dependent electrical relaxation in the materials. Further, at low frequencies the Z' values decrease with rise in tem-

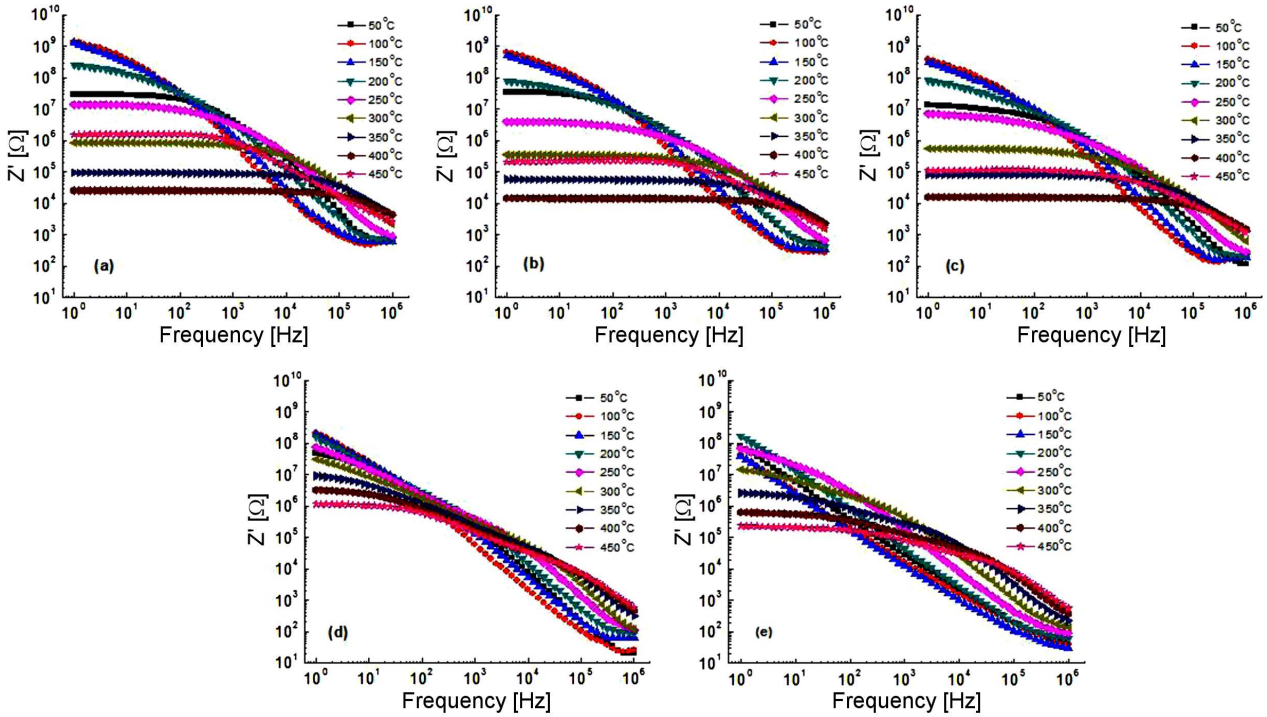

Figure 6. Variation of the real part of impedance with frequency of $Ba(In_{0.5}Nb_{0.5})_{1-x}Ti_xO_3$ ceramics: a) $x = 0$, b) $x = 0.25$, c) $x = 0.50$, d) $x = 0.75$ and e) $x = 1.0$ at different temperatures

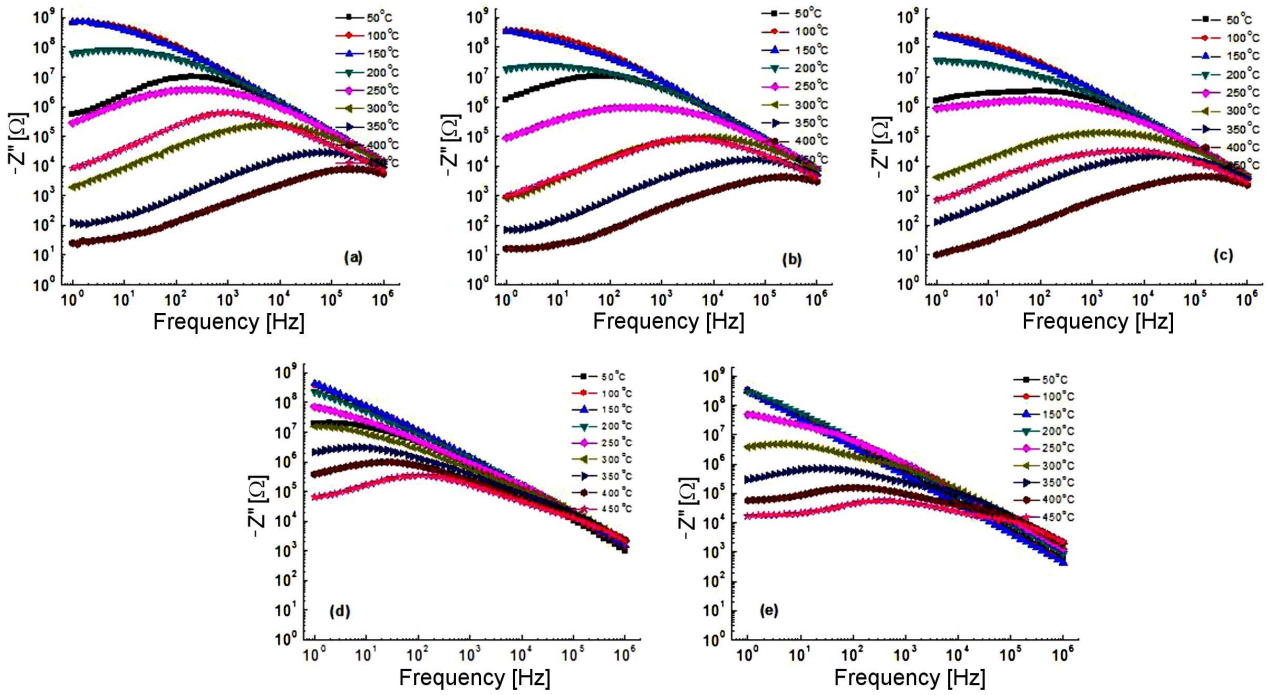

Figure 7. Variation of the imaginary part of impedance with frequency of $Ba(In_{0.5}Nb_{0.5})_{1-x}Ti_xO_3$ ceramics: a) $x = 0$, b) $x = 0.25$, c) $x = 0.50$, d) $x = 0.75$ and e) $x = 1.0$ at different temperatures

perature showing the negative temperature coefficient of resistance (NTCR) type behaviour of semiconductors. The relaxation time was estimated from the frequency at which Z''_{max} is observed. At the peak ($\omega = \omega_0$), the most probable relaxation is defined by the condition: $\omega \cdot \tau = 1$, where τ is the relaxation time and obeying the Arrhenius relationship:

$$\tau = \tau_0 \exp \frac{-U}{k_B \cdot T} \tag{3}$$

where τ_0, U, k_B and T are the pre-exponential factor, activation energy, Boltzmann constant and absolute temperature, respectively. The values of U were estimated using linear least square fit to the above equation and

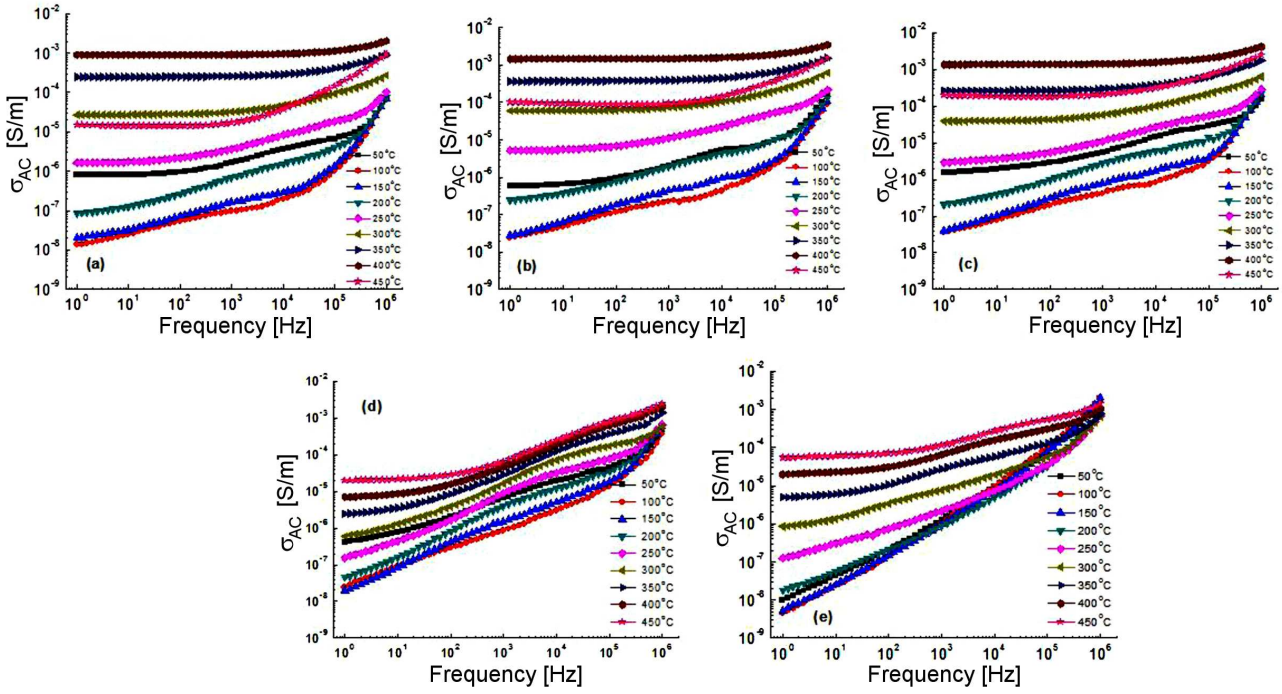

Figure 8. Variation of the AC conductivity with frequency of $Ba(In_{0.5}Nb_{0.5})_{1-x}Ti_xO_3$ ceramics: a) $x = 0$, b) $x = 0.25$, c) $x = 0.50$, d) $x = 0.75$ and e) $x = 1.0$ at different temperatures

data points. It is observed that partial replacement of pseudo-cation $(In_{0.5}Nb_{0.5})^{4+}$ with Ti^{4+}-ion led to the decrease in real and imaginary parts of impedance as well as activation energy.

Figure 8 shows the variation of AC conductivity (σ_{AC}) of the BINT ceramics as a function of frequency at different temperatures. The nature of variation of $\sigma_{AC}$with frequency exhibits dispersion throughout the chosen range of frequencies. Also, σ_{AC} increase with rise in frequency as well as temperature. Such increment in conductivity is due to the movement of thermal ions (generally comes from hopping motion of ions) from one preferable site to the other. The plots get flattened (low frequency plateau) upon further rise in temperature. The high-frequency conductivity dispersion may be attributed to the AC conductivity whereas the frequency independent plateau region of the conductivity pattern corresponds to the DC conductivity (σ_{DC}) of the material. The switch from frequency-independent to the frequency-dependent region shows the onset of the conductivity relaxation phenomenon which shifts to higher frequency side with the increase in temperature, indicating the translation from long range hopping to the short range ion-motion. Such dependence is associated with the displacement of carriers which move within the sample by discrete hops of length R between randomly distributed localized sites. Furthermore, the AC conductivity, in most of the materials due to localized states can be expressed using Jonscher's power law [25]: $\sigma_{AC} = \sigma_0 + A \cdot \omega^s$. The values of the index s were obtained from the slopes of the plots in the low frequency region, which always comes out to be less than 1 and are decreasing with the rise in temperature. This observation is consistent with correlated barrier hopping model [26]. Therefore, the electrical conduction in the BINT may be considered due to the short range translational type hopping of charge carriers. Besides, the value of s approaching zero at higher temperatures indicates that the DC conductivity dominates at higher temperatures in the low frequency region following the Jonscher's power law. It can be seen that the slope of the curves changes with changing temperature, which clearly indicates that the conduction process is dependent on both temperature as well as on frequency. Further, a decrease in the values of σ_{AC} is observed with the rise in temperature for all the compounds, thereby indicating the NTCR character of the samples. This may happen due to the accumulation of charge species at the barriers (grain boundaries) which get thermally activated, that plays a dominant role at elevated temperature showing NTCR characteristics. With the rise in temperature, these charge species have sufficient energy to jump over the barrier. Therefore, they are responsible for increasing the conductivity and hence the grain boundary resistance decreases beyond these temperatures.

Hopping type of electrical conduction is generally consistent with the existence of a high density of states in the materials having band gap like that of semiconductor. Due to the localization of charge carriers, formation of polarons takes place and the hopping conduction may occur between the nearest neighbouring sites. Figure 9 shows the variation of AC conductivity versus $10^3/T$ of the BINT ceramics at different frequencies. It is clear from all the plots that change in the slope of the curves at different temperature regions are different, which clearly indicates that carriers transport in

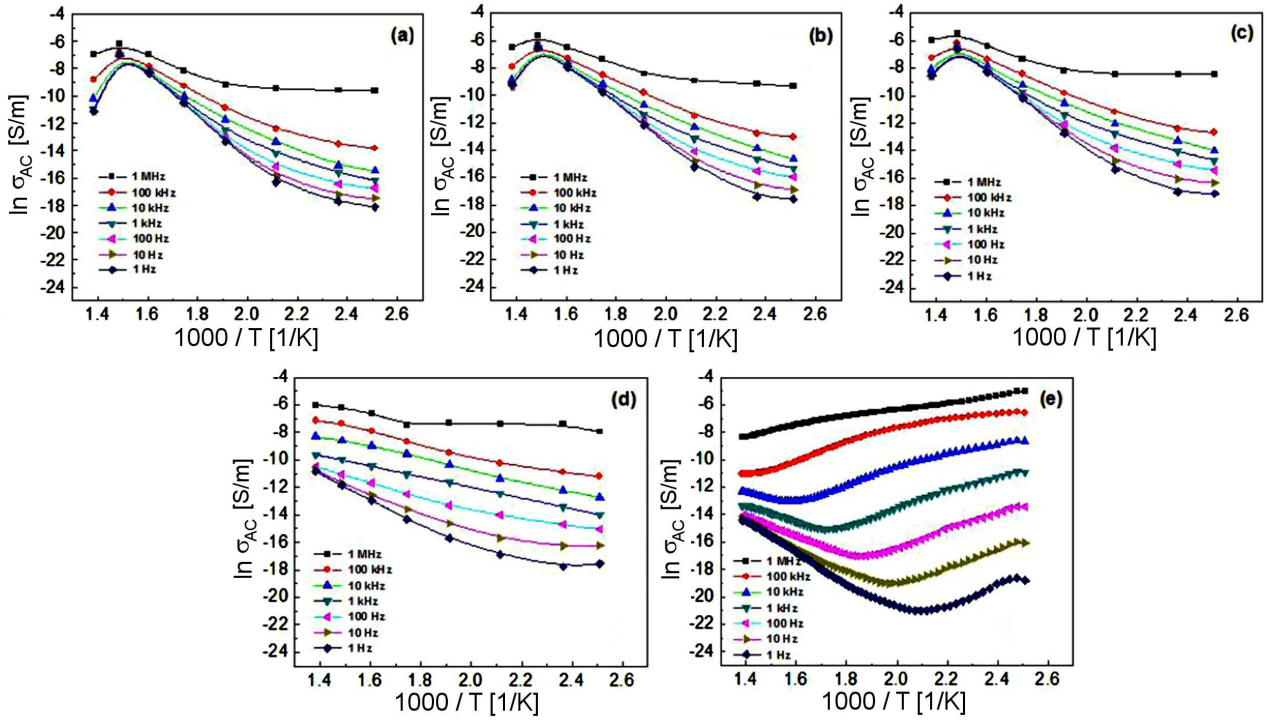

Figure 9. Variation of the real part of AC conductivity with temperature of $Ba(In_{0.5}Nb_{0.5})_{1-x}Ti_xO_3$ ceramics: a) $x = 0$, b) $x = 0.25$, c) $x = 0.50$, d) $x = 0.75$ and e) $x = 1.0$ at different frequencies

the samples are obeying the hopping type of conduction mechanism. The temperature dependent AC conductivity data, in high temperature region, were fitted to the Arrhenius relationship:

$$\sigma_{AC} = \sigma_0 \cdot \exp \frac{E_a}{k_B \cdot T} \tag{4}$$

where E_a is the apparent activation energy of conduction and T is the absolute temperature. It is observed that the values of σ_{AC} increase while the values of E_a decrease with increasing x. The low values of E_a might be due to the transport of charge carriers through hopping between localized states in a disordered manner [27].

It is observed (Fig. 9) that σ_{AC} increases with the rise in temperature for all the compounds under investigation, thereby indicating the negative temperature coefficient of resistance (NTCR) character of the samples. This may happen due to the accumulation of charges at the barriers which get thermally activated, that plays a dominant role at elevated temperature showing NTCR characteristics. With the rise in temperature, the charge species (which are accumulated at grain boundaries) have sufficient energy to jump over the barrier thereby increasing the conductivity. Thus, the grain boundary resistance decreases beyond these temperatures. On the other hand, a slight change in stoichiometry (i.e. the metal to oxygen ratio) in multi-metal complex oxides causes the creation of a large number of donor or accepter like states in the vicinity of conduction or valance bands. These donors or acceptors might be activated with less energy [28]. It is known that in perovskite titanates, ionization of oxygen vacancy creates conducting electrons, a process which can be described using the Kröger and Vink notation [29]. These excess electrons and oxygen vacancies are formed in the reduction reaction during sintering that enhances the electrical conductivity, dielectric loss and space charge accumulation at the grain boundaries which are detrimental to the material's performance [26,30]. It is reported that titanate based perovskite oxide materials contain Ti^{3+} that is formed because of the capturing of electrons released during the process of formation of oxygen vacancies by Ti^{4+}. The polaronic conduction of $3d$ electrons on Ti^{3+} with low mobility must be predominant at low temperature and these polaronic states are thermally dissociated and the residual carriers, $3d$ electrons, are strongly scattered by thermal phonons at high temperature, resulting in high electronic conductivity [31]. In BINT system, partial replacement of Ti^{4+} ions with In^{3+} and Nb^{5+} ions may result in localized oxygen vacancies and titanium vacancies given as:

$$12\,BaO + 3\,In_2O_3 + 2\,Nb_2O_5 + TiO_2 \longrightarrow$$
$$12\,Ba + Ti + 6\,In_{Ti} + 4\,Nb_{Ti} + 33\,O + 3\,V_O + V_{Ti}$$

where V_O and V_{Ti} are the oxygen and titanium vacancies, respectively. In_{Ti} and Nb_{Ti} represent the incorporation of In and Nb at Ti position, respectively. Since Ti can exist in +3 and +4 state, whereas Nb can exist in +3 and +5 states, Ti^{4+} and Nb^{5+} ions may capture the electrons to form Ti^{3+} and Nb^{3+} ions, respectively. The polaronic conduction of $3d$ electrons on Ti^{3+} and $4d$ electrons on Nb^{3+} with low mobility may be predominant at intermediate temperature. High electronic

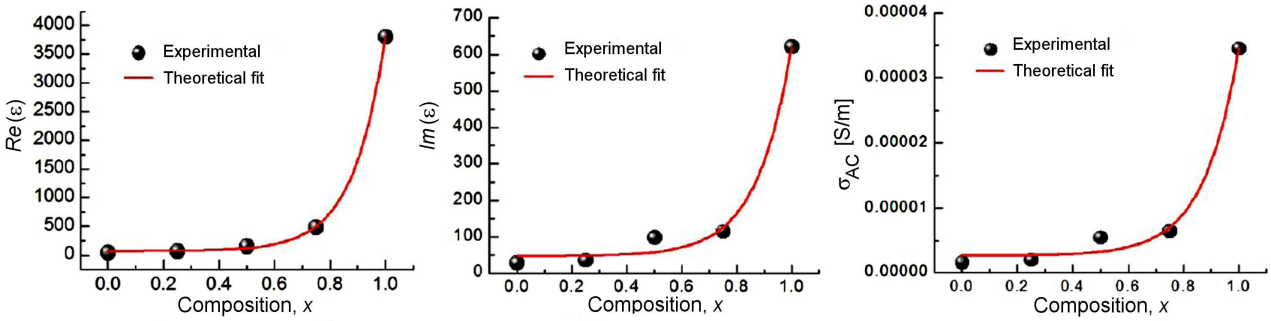

Figure 10. Variation of the real and imaginary parts of dielectric constant and the AC conductivity with composition (x) of $Ba(In_{0.5}Nb_{0.5})_{1-x}Ti_xO_3$ ceramics (points show experimental data and line shows theoretical fit)

Table 2. Concentration dependent variation of the real and imaginary parts of dielectric constant and the AC conductivity of $Ba(In_{0.5}Nb_{0.5})_{1-x}Ti_xO_3$ ceramics

Model	Parameters	ε'	ε''	σ_{AC}
$Y = Y_0 + A_0 \cdot e^{x/c}$	Y_0	69.87803	47.04451	2.6146×10^{-6}
	A_0	0.6639	0.20679	1.1493×10^{-8}
	c	0.11579	0.12614	0.12614
	r^2	0.99978	0.99121	0.99121

conductivity at elevated temperatures may also be attributed to the increase in polaronic conduction. This increase in polaronic conduction may be linked to the formation of more oxygen vacancies due to oxygen loss at very high temperatures. Contribution to the polaronic conduction from In-ion can be ruled out, as it has stable valence state (+3). In the present perovskite system, the high frequency localized orientation hopping may be attributed to the formation of dipoles, $Nb^{3+}-V_O$ and $Ti^{3+}-V'_O$. These dipoles can change their orientations by electron hopping. The hopping of 4*d* electrons, $Nb^{3+}-V_O$ and $Ti^{3+}-V'_O$, gives rise to localized energy levels in the energy gap of $Ba(In_{0.5}Nb_{0.5})_{1-x}Ti_xO_3$. The charge carriers trapped at these localized sites may form large polarons and conduction occurs as a result of thermally activated large polarons. This is also clear from the temperature dependence of s, which decreases with increasing temperature for hopping mechanism of large polarons [32,33].

Figure 10 shows the variation of the real and imaginary parts of dielectric constant and the AC conductivity with Ti-content (x) in $Ba(In_{0.5}Nb_{0.5})_{1-x}Ti_xO_3$ ceramics. It is seen that the values of ε', ε'' and σ_{AC} show an increasing trend with the increase in Ti-content. Further, ε', ε'' and σ_{AC} vs. Ti-content (x) data fit excellently well ($r^2 > 0.99$) with an exponential growth type of function given by: $Y = Y_0 + A_0 \cdot e^{x/c}$. Here Y_0, A_0 and c are material dependent constants where Y_0 and A_0 are the initial values (corresponding to $x = 0$) of these parameters. The values of these model parameters and constants are given in Table 2.

IV. Conclusions

$Ba(In_{0.5}Nb_{0.5})_{1-x}Ti_xO_3$ ceramics (BINT, where $x = 0$, 0.25, 0.50, 0.75 and 1.0) ceramics were synthesized using high temperature solid-state reaction method and sintered at 1400 °C/4 h (except for the pure $BaTiO_3$ which was sintered at 1300 °C/4 h). The unit cell structure of the BINT ceramics is observed to be cubic (*Pm3m*) up to $x = 0.50$ while for $x = 0.75$ and 1.0 it is tetragonal (*P4/mmm*). The unit cell volume decreases while the real and imaginary parts of dielectric constant as well as the AC conductivity increase with increasing Ti-content in the system. The variation of dielectric constant with temperature was found to be almost constant up to 100 °C ($T_{CC} \sim \pm10\%$) for $x = 0.50$ suggesting that this ceramics is suitable for capacitor applications. The ceramics showed the negative temperature coefficient of resistance character and supported the hopping type of conduction. The frequency dependence of the AC conductivity data obeyed Jonscher's power law. The real and imaginary parts of dielectric constant as well as AC conductivity data were fitted excellently well with the exponential growth type function.

Acknowledgements: The present work was supported by ER & IPR Division of Defense Research and Development Organization, New Delhi.

References

1. T.R. Shrout, S.J. Zhang, "Lead-free piezoelectric ceramics: Alternatives for PZT?", *J. Electroceram.*, **19** (2007) 111–124.
2. P.K. Panda, "Review: environmental friendly lead-free piezoelectric materials", *J. Mater. Sci.*, **44** (2009) 5049–5062.
3. J. Rödel, W. Jo, K.T.P. Seifert, E.-M. Anton, T. Granzow, D. Damjanovic, "Perspective on the development of lead-free piezoceramics", *J. Am. Ceram. Soc.*, **92** (2009) 1153–1177.
4. R.-A. Eichel, H. Kungl, "Recent developments and future perspectives of lead-free ferroelectrics", *Funct. Mater. Lett.*, **3** (2010) 1–4.

5. D. Damjanovic, N. Klein, J. Li, V. Porokhonskyy, "What can be expected from lead-free piezoelectric materials?", *Funct. Mater. Lett.*, **3** (2010) 5–13.
6. W. Li, J. Qi, Y. Wang, L. Li, Z. Gui, "Doping behaviors of Nb_2O_5 and Co_2O_3 in temperature stable $BaTiO_3$-based ceramics", *Mater. Lett.*, **57** (2002) 1–5.
7. Y. Yuan, S. Zhang, W. You, "Preparation of $BaTiO_3$-based X7R ceramics with high dielectric constant by nanometer oxides doping method", *Mater. Lett.*, **58** (2004) 1959–1963.
8. G. Li, S. Liu, F. Liao, S. Tian, X. Jing, J. Lin, Y. Uesu, K. Kohn, K. Saitoh, M. Terauchi, N. Di, Z. Cheng, "The structural and electric properties of the perovskite system $BaTiO_3$-$Ba(Fe_{1/2}Ta_{1/2})O_3$", *J. Solid State Chem.*, **177** (2004) 1695–1703.
9. Y. Hiruma, R. Aoyaqi, H. Nagata, T. Takenaka, "Piezoelectric properties of $BaTiO_3$-$(Bi_{1/2}K_{1/2})TiO_3$ ferroelectric ceramics", *Jpn. J. Appl. Phys. Part 1*, **43** (2004) 7556–7559.
10. S. Mahboob, A.B. Dutta, C. Prakash, G. Swaminathan, S.V. Suryanarayana, G. Prasad, G.S. Kumar, "Dielectric behaviour of microwave sintered rare-earth doped $BaTiO_3$ ceramics", *Mater. Sci. Eng. B*, **134** (2006) 36–40.
11. A. Umeri, T.A. Kuku, N. Scuor, V. Sergo, "Raman investigation of the ageing of Ni-$BaTiO_3$ multilayer ceramic capacitors", *J. Mater. Sci.*, **43** (2008) 922–926.
12. H.L.W. Chan, S.H. Choy, C.P. Chong, H.L. Li, P.C.K. Liu, "Bismuth sodium titanate based lead-free ultrasonic transducer for microelectronics wirebonding applications", *Ceram. Int.*, **34** (2008) 773–777.
13. K. Prasad, Priyanka, K.P. Chandra, A.R. Kulkarni, "Structural and electrical properties of lead-free perovskite ceramic: $Ba(In_{1/2}Nb_{1/2})O_3$", *J. Non-Cryst. Solids*, **357** (2011) 1209–1217.
14. K. Prasad, Powder diffraction file - Release 2012, International Centre for Diffraction Data, USA, 2012.
15. L.A. Khalam, H. Sreemoolanathan, R. Ratheesh, P. Mohanan, M.T. Sebastian, "Preparation, characterization and microwave dielectric properties of $Ba(B'_{1/2}Nb_{1/2})O_3$ [B′ = La, Pr, Nd, Sm, Eu, Gd, Tb, Dy, Ho, Y, Yb and In] ceramics", *Mater. Sci. Eng. B*, **107** (2004) 264–270.
16. E. Vlakhov, Y. Dimitriev, E. Gattef, A. Staneva, S. Aleksandrova, K. Nenkov, "Synthesis and superconducting properties of the composite in the system (1-x) $YBa_2Cu_3O_y$–x $Ba(Y_{1/2}Nb_{1/2})O_3$", *J. Mater. Sci. Lett.*, **16** (1997) 763–765.
17. S. Bhagat, K. Amar Nath, K.P. Chandra, R.K. Singh, A.R. Kulkarni, K. Prasad, "The structural, electrical and magnetic properties of perovskite (1-x) $Ba(Fe_{1/2}Nb_{1/2})O_3$–x $BaTiO_3$ ceramics", *Adv. Mater. Lett.*, **5** (2014) 117–121.
18. H. Yang, Y. Yang, Y. Lin, J. Zhu, F. Wang, "Preparation and electrical properties of (1-x) $Ba(Fe_{0.5}Nb_{0.5})O_3$–x $BaTiO_3$ ceramics", *Ceram. Int.*, **38** (2012) 1745–1749.
19. U. Intatha, S. Eitssayeam, K. Pengpat, G. Rujijanagul, T. Tunkasiri, "The structural and electrical properties of (1-x) $BaTiO_3$–x $BaFe_{0.5}Nb_{0.5}O_3$ ceramics", *Ferroelectr.*, **415** (2011) 176–181.
20. K. AmarNath, K. Prasad, "Structural and electric properties of perovskite $Ba(Sm_{1/2}Nb_{1/2})O_3$–$BaTiO_3$ ceramic", *Adv. Mater. Res.*, **1** (2012) 115–128.
21. K. Prasad, Priyanka, K. Amar Nath, K.P. Chandra, A.R. Kulkarni, "Dielectric relaxation in $Ba(Y_{1/2}Nb_{1/2})O_3$–$BaTiO_3$ ceramics", *J. Mater. Sci.: Mater. Electron.*, **25** (2014) 4856–4866.
22. J. Kumar, S.N. Choudhary, K. Prasad, R.N.P. Choudhary, "Electrical properties of 0.25 $Ba(Bi_{1/2}Ta_{1/2})O_3$–0.75 $BaTiO_3$", *Adv. Mater. Lett.*, **5** (2014) 106–110.
23. C.L. Tian, Z.X. Yue, Y.Y. Zhou, S.Q. Meng, "Structures and microwave dielectric properties of $Ba[Ti_{1-x}(Co_{0.5}W_{0.5})x]O_3$ (x = 0.40–0.90) perovskite ceramics", *J. Am. Ceram. Soc.*, **95** (2012) 1645–1650.
24. C. Tian, Z. Yue, Y. Zhou, L. Li, "Crystal structures and microwave dielectric properties of Zn,W co-substituted $BaTiO_3$ perovskite ceramics", *J. Solid State Chem.*, **197** (2013) 242–247.
25. A.K. Jonscher, *Dielectric Relaxation in Solids*, Chelsea, New York, 1983.
26. S. Bhagat, K. Prasad, "Structural and impedance spectroscopy analysis of $Ba(Fe_{1/2}Nb_{1/2})O_3$ ceramic", *Phys. Status Solidi (a)*, **207** (2010) 1232–1239.
27. K. Prasad, C.K. Suman, R.N.P. Choudhary, "Electrical characterization of $Pb_2Bi_3SmTi_5O_{18}$ ceramic using impedance spectroscopy", *Adv. Appl. Ceram.*, **105** (2006) 258–264.
28. R.C. Buchanan, *Ceramic Materials for Electronics*, Marcel Dekker, New York, 1986.
29. F.A. Kröger, H.J. Vink, "Relations between the concentrations of imperfections in crystalline solids", *Solid State Phys.*, **3** (1956) 307–435.
30. R. Maier, J.L. Chon, J.J. Neumeier, L.A. Bendersky, "Ferroelectricity and ferrimagnetism in iron-doped $BaTiO_3$", *Appl. Phys. Lett.*, **78** (2001) 2536–2539.
31. E. Iguchia, S. Mochizuki, "Electric conduction and dielectric relaxation processes in solid oxide fuel cell electrolyte $La_{0.5}Sr_{0.5}Ga_{0.6}Ti_{0.4}O_{3-\delta}$", *J. Appl. Phys.*, **96** (2004) 3889–3896.
32. S.R. Elliott, "A.c. conduction in amorphous chalcogenide and pnictide semiconductors", *Adv. Phys.*, **36** (1987) 135–217.
33. S. Upadhyay, A.K. Sahu, D. Kumar, O. Parkash, "Probing electrical conduction behavior of $BaSnO_3$", *J. Appl. Phys.*, **84** (1998) 828–833.